Acta Scientiarum
http://periodicos.uem.br/ojs/acta
ISSN on-line: 1807-8664
Doi: 10.4025/actascitechnol.v47i1.71350



# Numerical modeling of reinforced concrete sandwich panels with EPS core under compression

**Geovany Ferreira Barrozo[1*], William Taylor Matias Silva[1] and Luciano Mendes Bezerra[1,2]**

[1]Departamento de Engenharia Civil e Ambiental, Universidade de Brasília, Via L3 Norte, Asa Norte, 70910-900, Brasília, Distrito Federal, Brasil. [2]Programa de Pós-Graduação em Integridade de Materiais de Engenharia, Universidade de Brasília, Brasília, Distrito Federal, Brasil. *Author for correspondence. E-mail: geovany.sh75@gmail.com

**ABSTRACT:** The application of sandwich panels has grown significantly in Brazilian civil construction recently, with greater use in residential buildings. Nevertheless, in the abcsence of regulatory standards and reliable calculation methodology, these construction elements are frequently employed without a genuine comprehension of their structural performance. Therefore, in order to evaluate the structural behavior of these panels when subjected to compression loads, a 3D nonlinear finite element model was developed using ABAQUS (2014) software. This study presents a numerical investigation, detailing the geometry of the Sandwich Panel model, the types of meshes and finite elements used in the modeling, as well as the approach employed to model material contact interactions and simulate boundary conditions and loading applications. Additionally, this study used the Concrete Damaged Plasticity Model (CDPM) from the ABAQUS library to model concrete. It also shows the plastic input parameters and formulations of the constitutive laws used to describe the uniaxial behavior of concrete under tension and compression. It also explains the methodology for calculating the evolution of the damage variables. For the modeling of steel and expanded polystyrene (EPS), the constitutive models PLASTIC and ELASTIC from ABAQUS library were used. The developed model satisfactorily simulated the structural behavior of sandwich panels subjected to eccentric compression loads, making it reliable for estimating their strength capacity.

**Keywords:** ABAQUS; finite element; CDPM; strength capacity; structural behavior.

Received on January 01, 2024.
Accepted on February 28, 2025.

## Introduction

Sandwich panels comprise structural elements composed of layers, as illustrated in Figure 1. For their conception, different materials may be used. In particular, concrete panels find widespread use as sealing components and bearing walls. They are also suitable for application in floors, slabs, and roofs. According to the PCI Committee Report (2011), precast concrete sandwich panels are manufactured by arranging two layers of concrete connected to another central layer of rigid foam plastic insulation. To ensure the appropriate connection of these parts, elements known as connectors are used.

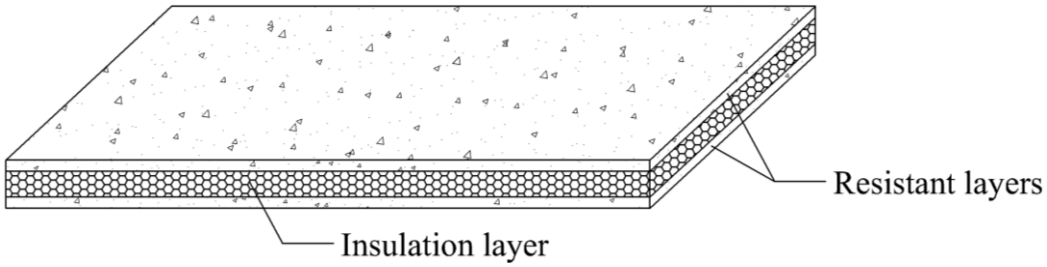


**Figure 1.** Sandwich panel.

The use of sandwich panels for housing construction can offer several advantages compared to conventional construction techniques. These benefits include improved thermal and acoustic insulation, lighter structural components, the possibility of creating monolithic structures with higher rigidity, ease of transportation and handling, on-site molding with form elimination, reduced need for specialized labor, lower costs, and faster execution. As a result of these characteristics, the popularity of construction systems

employing sandwich panels with an EPS core for building construction has been observed in various countries, such as Bangladesh, Singapore, China, India, Indonesia, Malaysia, Egypt, Venezuela, and Brazil (Bertini & Pinheiro, 2007).

The intricate structural behavior of sandwich panels, attributed to the nonlinearity of their materials and the inherent uncertainties in the interaction among diverse components, has led researchers to rely on experimental investigations and simplified analytical hypotheses. Furthermore, the scarcity of information regarding the behavior of these structural elements is attributed to the high cost of full-scale tests and the significant challenges in fabricating reduced-scale models (Benayoune et al., 2006).

Finite Element Method (FEM) numerical analyses have become an increasingly common approach to studying the behavior of structural components that cannot be easily tested, such as sandwich panels (Chen et al., 2015). Consequently, it allows for preliminary numerical investigations into the structural behavior of the element and facilitates the selection of specific regions of interest for the study. This enhances the efficiency of quantifying and installing measurement instruments to serve the research objectives better, thus reducing the number of test elements (Santana et al., 2020).

In this context, the development of reliable numerical models for analyzing and elucidating the structural behavior of sandwich panels can serve as a foundation for establishing design guidelines (Huang & Hamed, 2019). Thus, the creation of a nonlinear numerical model using the FEM that is dependable is essential to support experimental results, assess the feasibility of further studies, and validate the mechanical behavior of reinforced concrete sandwich panels. Moreover, the utilization of three-dimensional numerical models, as opposed to simplified models, allows for highlighting the influence on the structural response of the sandwich panel components through more detailed analyses of the interaction among internal panel components (Serpilli et al., 2021).

This research is guided by the significance of numerical analysis in understanding the mechanical behavior of sandwich panels subjected to compression loads. Thus, the objective is to perform numerical simulations using the FEM by developing a three-dimensional numerical model of a reinforced concrete sandwich panel with an EPS core and straight connectors made of steel. The model will consider the non-linear behavior of the materials involved.

## Material and methods

In this study, a Finite Element (FE) model was developed using the ABAQUS software, drawing upon the well-established experience from previous research with similar numerical studies as done by Chen et al. (2015), Hopkins et al. (2017), Lima et al. (2020), Lima et al. (2022), Santana et al. (2020). The design of the sandwich panel model involved separate modeling of the concrete layers, the EPS layer, the welded steel wire meshes (here after called wire), and the steel reinforcement bars. Furthermore, the FE numerical simulations considered the non-linear behavior of concrete and the contact interactions between the sandwich panel layers.

The FE model's geometry was based on the test specimens developed in the experimental work by Gara et al. (2012), where reinforced concrete sandwich panels with wire meshes and an EPS insulation layer were subjected to compression tests. In their study, the tested panels had a total length of 2940 mm, a width of 1120 mm, and varying thicknesses depending on the type of test specimen. The concrete layers had a thickness of 35 mm, while the thickness of the EPS layer varied.

In the current study, the WP08, WP12, and WP16 panels were modeled, with insulation layer thicknesses (c) of 80 mm, 120 mm, and 160 mm, respectively. This resulted in corresponding total thicknesses (h) of 150 mm, 190 mm, and 230 mm. Additionally, each experimental model featured concrete beams with a height of 120 mm at their ends. These beams were reinforced with longitudinal 8 mm diameter bars and transverse 6 mm diameter bars spaced at 200 mm, as illustrated in Figure 2.

Furthermore, as shown in Figure 2, each panel contained wire meshes made of steel wires with a diameter of 3 mm, placed within the concrete layers and interconnected by straight steel connectors, also with a diameter of 3 mm. These straight connectors passed through the EPS layer and were welded to the steel wire meshes at their ends - see Section A-A in Figure 2.

For the molding of the panels, Gara et al. (2012) used ready-mixed concrete with sand of a maximum diameter not exceeding 3 mm, along with additives to enhance adhesion and workability. So, to determine the mechanical properties of the concrete and steel used in the panel production, uniaxial compression tests were conducted (Gara et al., 2012) on cylindrical specimens to obtain the average compressive strength ($f_{cm}$)

and tensile strength ($f_{tm}$) of the concrete. Moreover, characterization tests were performed on the steel used in the wire meshes and connectors to determine its average tensile strength ($f_m$) and percentage elongation at rupture ($A_{gt}$), as specified in (Table 1).

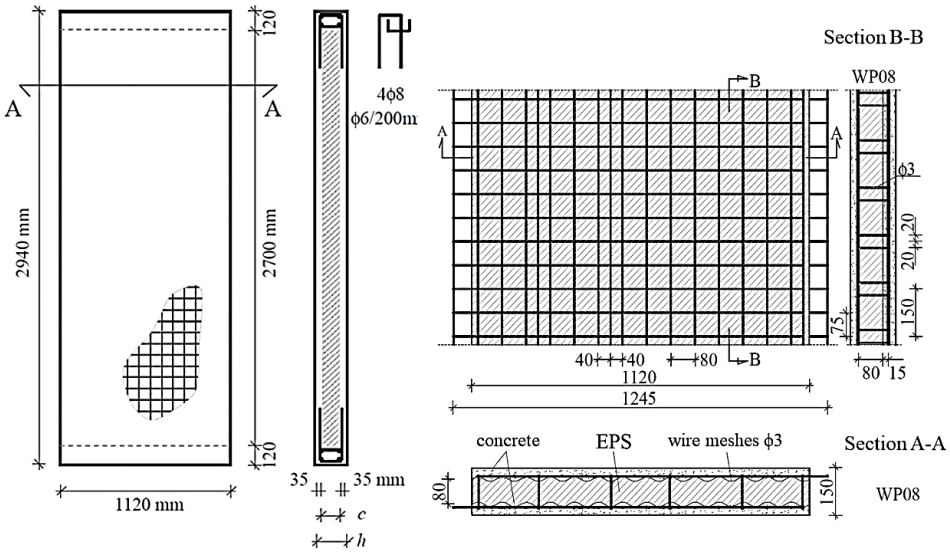


**Figure 2.** The geometry of the experimental models for compression tests (Gara et al., 2012).

**Table 1.** Properties of the concrete and steel for wire mesh.

| Concrete | Wire Mesh |
|---|---|
| $f_{cm}$ = 25.10 MPa | $f_m$ = 769.00 MPa |
| $f_{tm}$ = 2.40 MPa | $A_{gt}$ = 7.62 % |

Figure 3 illustrates the experimental setup for the eccentric compression tests by Gara et al. (2012). In his arrangement, the concrete beams were confined by metal profiles to ensure that the lower end of the panel, positioned on a roller, remains pinned. Furthermore, the upper end of the panel is clamped to prevent lateral displacement.

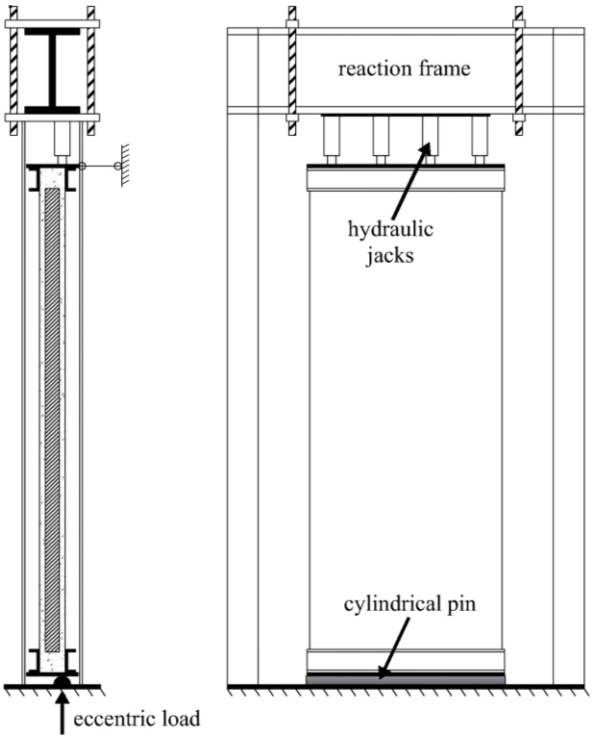


**Figure 3**. Experimental setup for the compression tests (Gara et al., 2012).

The tests are conducted with load control, where the loading is applied by four hydraulic jacks with a maximum capacity of 500 kN, positioned on a steel plate responsible for distributing the load onto the upper reinforced concrete beam. The load is applied along the axis of one of the concrete layers. Additionally, LVDTs (Linear Variable Differential Transducers) are installed to monitor horizontal displacements at mid-thirds and mid-height of the panel, as well as the slipping and separation between the concrete layers and deformation at mid-height.

The model was developed in ABAQUS and subdivided into parts based on the type of material and geometry, such that each part was individually modeled with independent FE meshes. The FEs employed in the modeling are available in the ABAQUS library and are suitable for this type of analysis, which involves nonlinearities, contact interactions, large deformations, plasticity, and damage.

The EPS insulation layer of the sandwich panel was modeled with C3D8R hexahedral elements with 8 nodes, reduced integration, and a 30 mm size. According to the ABAQUS User's Manual, this type of FE is based on the Lagrangian formulation, in which the element deforms with the material. Reduced numerical integration is employed, which exhibits lower sensitivity to element distortion and yields more accurate results at a reduced computational cost. The modeling took into account the EPS´s wavy cross-section and the holes in the insulation layer where the connectors go through, as shown in Figure 4.

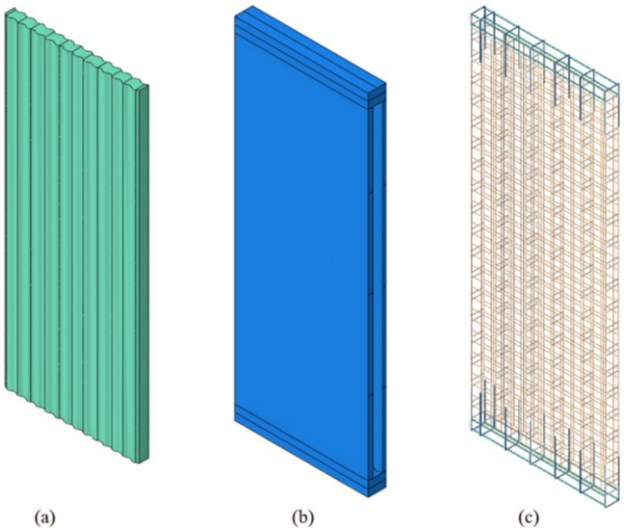


**Figure 4.** (a) EPS part; (b) Concrete part; (c) Metal part.

For the concrete part of the panel, including the two resistant layers and the end beams, a FE mesh composed of C3D8R elements with a size of 30 mm was also used. The resistant layers were appropriately modeled to fit the wavy surface of the EPS layer. Furthermore, truss elements (T3D2) with a Lagrangian formulation, two nodes, and three degrees of freedom at each node were used to model the wire meshes, straight connectors, and reinforcement bars of the beams. The size of the elements used was 30 mm for diameters of 3 mm of wire meshes and connectors and for the stirrups of 6 mm and for beams' reinforcement bars of 8 mm, as presented in Figure 4.

Figure 5 presents the FE mesh configuration used for each part of the numerical model. Table 2 shows the total number of nodes and finite elements that were used to model all of the WP08 test specimen's sections. The average processing time required for this FE mesh configuration was 8 hours, utilizing a computer equipped with an Intel Core i7-10700F processor operating at a frequency of 2.9 Gigahertz and 16 Gigabytes of RAM.

The contact interaction between the EPS insulation layer and the internal surfaces of the concrete part, composed of the resistant layers and the end beams, was simulated using the *surface-to-surface* contact interaction. The conception of mechanical restraints was based on the *kinematic contact method*. Regarding the tangential behavior properties, a *penalty* friction formulation with a friction coefficient of 0.1 was assigned. Additionally, the so-colled *hard* property in ABAQUS was considered for preventing one surface from penetrating the other.

For the interaction between concrete and the wire meshes, connectors, and reinforcement bars of the beams, the *embedded* constraint was used. This method ensures that the wire, connectors, bars, and concrete move together without relative displacement. The *embedded* constraint avoids slipping between those

elements. No contact interaction was considered between the connectors and the EPS layer; holes were modeled in the insulation layer at the locations where the connectors pass through.

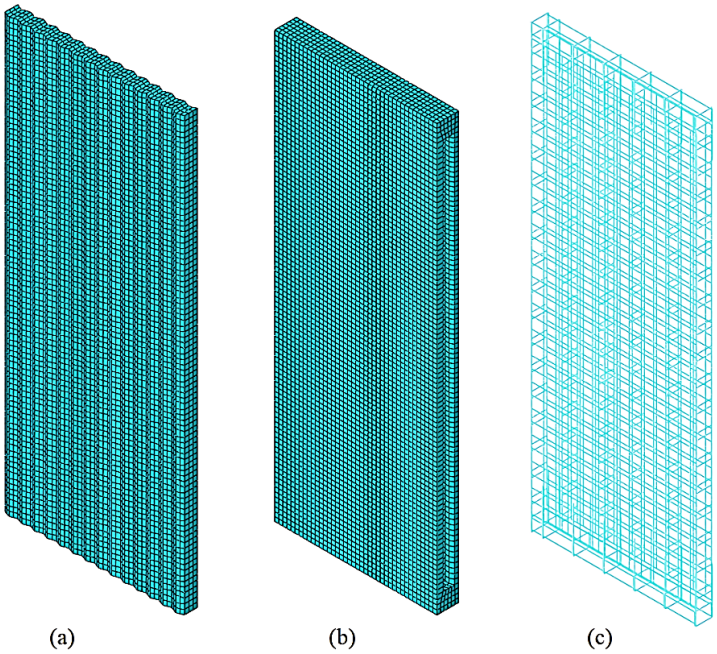


**Figure 5.** FE Mesh of (a) Concrete Part; (b) EPS Part; (c) Metal Part.

**Table 2**. FE mesh configuration and finite element setup of the model.

| Parts of the model | Element type | Number of elements | Number of nodes |
|---|---|---|---|
| Resistant layers and beams | C3D8R | 9120 | 17466 |
| EPS layer | C3D8R | 15120 | 20748 |
| Wire meshes and connectors | T3D2 | 7564 | 6198 |
| Reinforcement of the beams | T3D2 | 792 | 828 |

In this case, it is understood that modeling the EPS layer may not be indispensable. Nevertheless, it is crucial to consider this layer and understand its primary function as a filling material that separates the concrete layers. This filler ensures that the moment of inertia of the concrete sections goes up. This feature makes the panel stronger and more resource-efficient. The EPS filler also improves the insulation properties of the sandwich panels.

The model's boundary conditions applied on the FE model reproduced the support and load conditions used in the experimental test (Gara et al., 2012), as can be seen in Figure 3. Accordingly, constraints were assigned to the upper and lower surfaces of the panel, limiting the displacements and rotations. Figures 3 and 6 show the boundary conditions. Accordingly, some *rigid body* constraints were assigned to the upper and lower surfaces of the panel.

A reference point was designated to simulate the support constraints on the lower surface of the panel. At this point, displacements in the X, Y, and Z directions were restricted to reproduce the effect of confinement provided by the steel profiles on the lower beam. Rotations around the Y and Z axes were also restricted, allowing only rotation around the X axis to simulate the effect of the roller above, which the panel is positioned in the test system, as illustrated in Figure 6. The reference point is also located along the axis of one of the resistant layers for the eccentric compression test. The boundary conditions are detailed in Figure 6, considering that $U_k$ represents a displacement along axis-k and $R_j$ is a rotation around axis-j.

Regarding the boundary conditions at the upper part of the panel, a reference point was selected where displacements in the X and Z directions and rotation around the X-axis were constrained to simulate horizontal clamping and confinement of the steel profiles on the upper beam in the testing system. Additionally, the load was applied at the same reference point to ensure even distribution over the top surface of the panel, as can be seen in Figure 6. Therefore, $Q_y$ is applied at the top nodes of the panel (see Figure 6 and the hydraulic jacks in Figure 3).

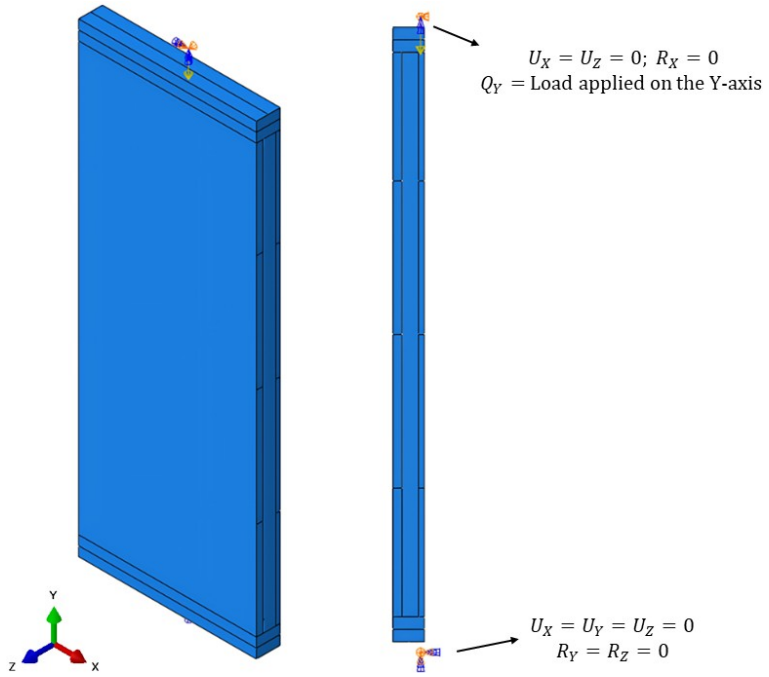


**Figure 6.** Boundary and loading conditions.

The analysis method employed in this study was the *dynamic explicit* method. This method is suitable for analyses involving dynamic loadings but can also be applied to static analyses with monotonic loadings. For that, the inertial effects must be minimized by using a sufficiently small loading application rate. In this research, an average loading application rate generating a displacement of 4.15 mm $s^{-1}$ was used. This rate kept the kinetic energy during the analysis below 5% of the internal energy. Several authors have used this method for static analyses and achieved good results, including Bezerra et al. (2018), Chen et al. (2015), Hopkins et al. (2017), Goh et al. (2016), Lima et al. (2022) and Santana et al. (2020).

The analyses conducted in this study were automatically terminated by the software, always using the ABAQUS (2020) standard stopping criterion. The application of this standard stopping criterion does not render it impossible to achieve satisfactory results, as the stop consistently occurred after the panel rupture had already occurred. Consequently, it was possible to compare experimental and numerical results to determine stresses and displacements at the moment of failure.

In this study, the *Concrete Damaged Plasticity Model* (CDPM) was used to model the resistance of the concrete layers and end beams of the sandwich panel. This constitutive model, available in ABAQUS, was developed by Lubliner et al. (1989) and Lee and Fenves (1998). It is considered ideal for simulating concrete behavior, as it is a continuous damage model based on plasticity theory. The CDPM accounts for failure mechanisms such as tensile cracking and compressive crushing (Alfarah et al., 2017).

Several authors have obtained satisfactory results by modeling concrete using the CDPM as Bezerra et al. (2018), Chen et al. (2015), Hopkins et al. (2017), Goh et al. (2016), Lima et al. (2020), Lima et al. (2022), and Santana et al. (2020). To simulate concrete with the CDPM, plastic parameters, uniaxial tensile and compressive behavior, and damage variable evolution must be specified. In this research, the average compressive and tensile strengths were considered as 25.10 MPa and 2.40 MPa, respectively (Gara et al., 2012). A Poisson's ratio of 0.2 and a concrete density of 2400 kg m-3 were also used.

Plastic parameters are variables that influence the yield criterion and the plastic flow rule (hyperbolic Drucker-Prager function) of the CDPM. Such parameters are defined as (1) the dilatancy angle, (2) the ratio between the tensile and compressive shear stress, (3) the ratio between biaxial and uniaxial compressive stresses that define the onset of non-linear behavior, and (4) the eccentricity of the plastic potential surface. In this study, the parameters specified from (1) to (4) were 13°, 0.7, 1.16, and 0.1, respectively (Alfarah et al., 2017).

The law defining the uniaxial compressive behavior adopted in this study was proposed by Feenstra (1993) and used by other authors (Serpilli et al., 2021; Clementi et al., 2018; Angiolilli & Gregori, 2020). These authors achieved favorable results in modeling ready-mixed concrete, masonry, and mortar. Figure 7 presents the uniaxial compressive behavior of concrete adopted in this research.

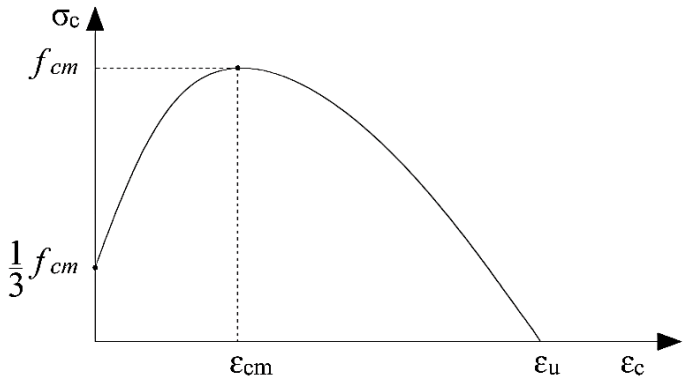


**Figure 7.** Uniaxial behavior of concrete under compression.

Thus, the stress-strain curve ($\sigma_c \; x \; \varepsilon_c$) that describes this concrete compression behavior is determined from Equations 1-4:

$$\sigma_c = \begin{cases} \frac{f_{cm}}{3}\left(1 + 4\frac{\varepsilon}{\varepsilon_{cm}} - 2\frac{\varepsilon^2}{{\varepsilon_{cm}}^2}\right) \; se \; \varepsilon < \varepsilon_{cm} \\ f_{cm}\left(1 - \frac{(\varepsilon - \varepsilon_{cm})^2}{(\varepsilon_u - \varepsilon_{cm})^2}\right) \; se \; \varepsilon_{cm} \leq \varepsilon < \varepsilon_u \end{cases} \quad (1)$$

$$\varepsilon_{cm} = \frac{4f_{cm}}{3E_{ci}} \quad (2)$$

$$\varepsilon_u = 1.5\frac{G_{ch}}{l_{eq} \cdot f_{cm}} - \frac{11}{48}\varepsilon_{cm} \quad (3)$$

$$G_{ch} = \left(\frac{f_{cm}}{f_{tm}}\right)^2 \cdot G_F \quad (4)$$

Where $f_{cm}$ is the average compressive strength of concrete, $\varepsilon_{cm}$ corresponds to the strain at the average compressive strength, $\varepsilon_u$ is the ultimate strain. According to the recommendations of the *Fédération Internationale du Béton* (Fédération Internationale du Béton [FIB], 2013), $E_{ci}$ is the initial elastic modulus, $E_{ci} = \alpha_E \cdot 10000 \cdot {f_{cm}}^{1/3}$, and $f_{cm} = f_{ck} + 8$ (in MPa), where $f_{ck}$ is the characteristic compressive strength, and $\alpha_E$ is a coefficient assigned based on the type of aggregate. In this research, a value of 0.7 is adopted for sandstone aggregates, which is more suitable for modeling ready-mixed concrete. Additionally, $G_{ch}$ (N/mm) represents the concrete crushing energy, and $l_{eq}$ corresponds to the equivalent length of the finite element. Equation 4 was proposed by [FIB] (2013), where $G_F$ (N/mm) is the fracture energy and $f_{tm}$ (MPa) corresponds to the average tensile strength of concrete, with $G_F = 0.073 \cdot {f_{cm}}^{0.18}$ and $f_{tm} = 0.3016 \cdot {f_{ck}}^{2/3}$.

The uniaxial tensile behavior of concrete, illustrated in Figure 8, presents a stress-strain curve ($\sigma_t \; x \; \varepsilon_t$) that is subdivided into two stages. The first stage is linear and described by $E_0\varepsilon_t$, where $E_0 = E_{ci}(0.8 + 0.2\, f_{cm}/88)$ (in MPa), which, according to the [FIB] (2013), represents the secant modulus. The second stage of *softening* is determined by the exponential function proposed by Cornellissen et al. (1986), as used in the research of Alfarah et al. (2017), which relates the concrete's tensile strength to the critical crack opening, as described by Equations 5-7:

$$\frac{\sigma_t(w)}{f_{tm}} = \left[1 + \left(c_1 \cdot \frac{w}{w_c}\right)^3\right] \cdot e^{-c_2\frac{w}{w_c}} - \frac{w}{w_c} \cdot (1 + {c_1}^3) \cdot e^{-c_2} \quad (5)$$

$$w_c = 5.14 \cdot \frac{G_F}{f_{tm}} \quad (6)$$

$$\varepsilon_t = \varepsilon_{tm} + \frac{w}{l_{eq}} \quad (7)$$

Where $w$ and $w_c$ correspond to crack opening and critical crack opening, respectively, and $\varepsilon_{tm}$ represents the strain related to the average tensile strength. Furthermore, the authors Cornelissen et al. (1986) proposed the dimensionless parameters $c_1 = 3$ and $c_2 = 6.93$. Additionally, in Figure 8, $d_t$ is the tensile damage variable, ${\varepsilon_t}^{pl}$ and ${\varepsilon_t}^{el}$ are defined as the plastic and elastic strain components damaged in tension, while ${\varepsilon_t}^{ck}$ and ${\varepsilon_{0t}}^{el}$ correspond to the cracking strain and undamaged elastic strain, respectively.

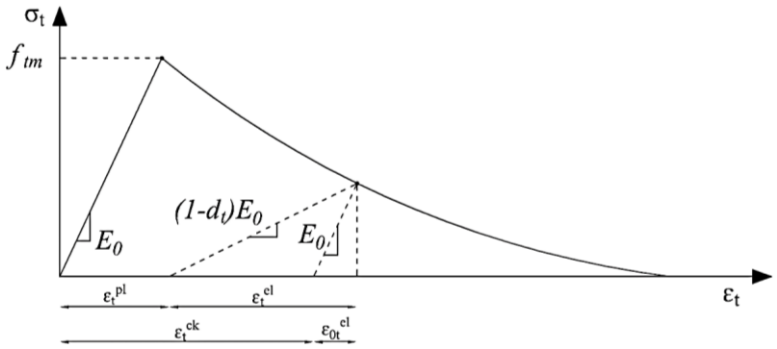


**Figure 8**. Uniaxial tensile behavior of concrete.

The methodology employed to calculate the damage variables in this study was developed by Alfarah et al. (2017). The compression damage ($d_c$) and tensile damage ($d_t$) are defined using Equations 8-11:

$$d_c = 1 - \frac{1}{2+a_c}\left[2(1+a_c)e^{(-b_c\varepsilon_c{}^{ch})} - a_c e^{(-2b_c\varepsilon_c{}^{ch})}\right] \quad (8)$$

$$d_t = 1 - \frac{1}{2+a_t}\left[2(1+a_t)e^{(-b_t\varepsilon_t{}^{ck})} - a_t e^{(-2b_t\varepsilon_t{}^{ck})}\right] \quad (9)$$

$$b_c = \frac{1.97(f_{ck}+8)}{G_{ch}} l_{eq} \quad (10)$$

$$b_t = \frac{0.453 {f_{ck}}^{2/3}}{G_F} l_{eq} \quad (11)$$

Where $\varepsilon_c{}^{ch} = \varepsilon_c - \sigma_c/E_0$ corresponds to the plastic crushing strain, $\varepsilon_t{}^{ck} = \varepsilon_t - \sigma_t/E_0$ corresponds to the cracking strain, $a_c = 7.873$, and $a_t = 1$.

The present study employed a constitutive model available in the ABAQUS library, named PLASTIC. This model is formulated as an elastoplastic model, taking into account the Von Mises yield criterion through an associative plastic flow rule. The uniaxial behavior of the steel is simulated using a trilinear curve proposed by Nguyen and Kim (2009), as shown in Figure 9. The yield stress ($\sigma_y$) is determined at a strain of 0.2% ($\varepsilon_y$), and the ultimate stress ($\sigma_u$) is reached at a strain of 0.6% ($\varepsilon_u$).

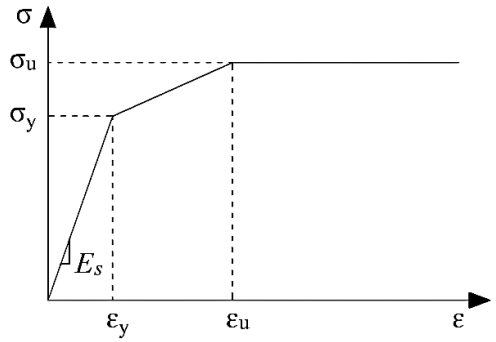


**Figure 9.** Uniaxial behavior of the steel.

Furthermore, in this study, the average tensile strength obtained from the tests conducted by Gara et al. (2012) was assigned to the wire meshes and connectors. For the reinforcement of the beams, the specifications of BS EN 4449:2005 for class B500B were utilized, considering the characteristic tensile properties. The remaining parameters adopted are listed in Table 3.

**Table 3.** Properties used for steel modeling.

| Component | Density (kg m$^{-3}$) | Young's modulus (MPa) | Poisson's ratio | $\sigma_y$ (MPa) | $\sigma_u$ (MPa) |
|---|---|---|---|---|---|
| Wire meshes and connectors | 7850 | 210000 | 0.3 | 600 | 769 |
| Reinforcement bars the beams | 7850 | 210000 | 0.3 | 500 | 540 |

The constitutive model used for EPS in this study is available in the ABAQUS library and is referred to as *ELASTIC*. This model assumes a linear elastic behavior with isotropic properties for the material. Such an

approach for EPS modeling has also been employed by other researchers who developed numerical models for sandwich panels such as Huang and Hamed (2019), Serpilli et al. (2021), Hopkins et al. (2017), Chen et al. (2015), and Goh et al. (2016). In this study, the mechanical properties adopted for EPS modeling are based on the model proposed by Serpilli et al. (2021), which includes a density of 15 kg $m^{-3}$, a Poisson's ratio of 0.12, and Young's modulus of 6.5 MPa.

As observed in Gara et al. (2012), considering the high stiffness of the concrete layers compared to the EPS layer, the EPS can be assumed to deform elastically. The EPS layer strength is negligible; its main function is to fill the space in between the concrete layers and provide thermal and acoustic insulation.

## Results and discussion

As explained earlier, the numerical model was validated based on the experimental tests carried out by Gara et al. (2012). Three models of reinforced concrete sandwich panels with welded wire meshes and EPS insulation were tested. The tests differ from each other in the thickness of the EPS insulation layer. The models WP08, WP12, and WP16 had insulation layers with thicknesses of 80, 120, and 160 mm, respectively. Each panel was subjected to eccentric compression tests, with two tests conducted for each experimental model. A set of hydraulic jacks applied the load, producing lateral deflection at the mid-height of the sandwich panels; see Figure 3.

The strength capacity of the sandwich panels was assessed by measuring the ultimate load and the lateral deflection, as illustrated in Figure 10. Figure 10 shows the curves load vs. deflection at the mid-height of the panel for both the experimental and numerical models. A good agreement is observed between the experimental and numerical load-deflection curves.

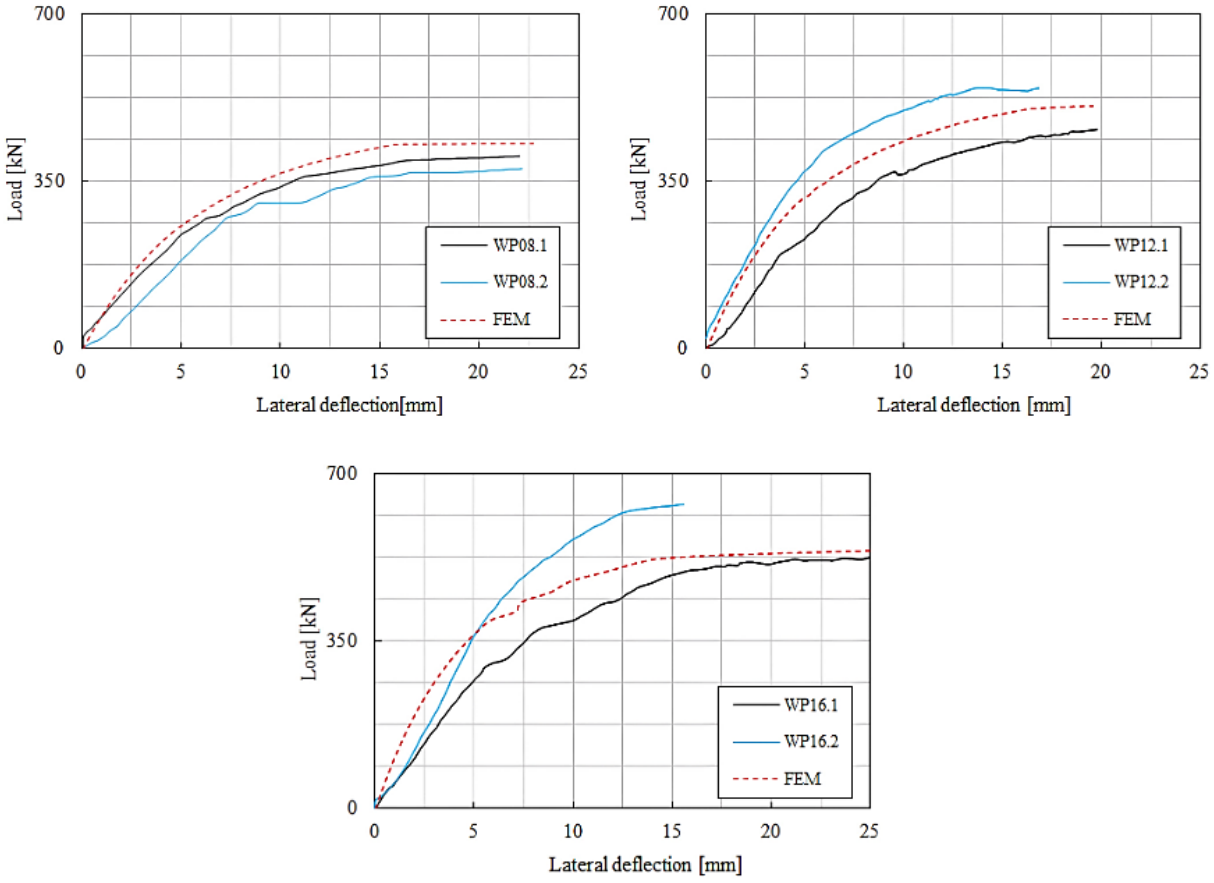


**Figure 10.** Load-deflection curves at the mid-height of the panel.

The results are presented in Table 4 for the ultimate load and lateral deflection at the point of failure, located at the mid-height of the panel. In that table, $P_{exp}$ and $P_{FEM}$ represent, respectively, the experimental and numerical ultimate loads. Additionally, $d_{exp}$ and $d_{FEM}$ correspond to the experimental and numerical lateral deflections, respectively.

**Table 4.** Results for lateral load-deflection.

| Specimens | $d_{exp}$(mm) | $d_{FEM}$ (mm) | $P_{exp}$(kN) | $P_{FEM}$ (kN) | $P_{exp}/P_{FEM}$ |
|---|---|---|---|---|---|
| WP08.1 | 22.00 | 22.69 | 401.00 | 429.54 | 0.93 |
| WP08.2 | 22.15 | | 375.00 | | 0.87 |
| WP12.1 | 19.79 | 19.58 | 460.00 | 507.95 | 0.91 |
| WP12.2 | 16.87 | | 545.00 | | 1.07 |
| WP16.1 | 25.09 | 25.53 | 524.00 | 540.10 | 0.97 |
| WP16.2 | 15.54 | | 630.00 | | 1.17 |

In Table 4, the average of $P_{exp}/P_{FEM}$ is 0.987 with a coefficient of variation of 0.113. Therefore, it can be asserted that the developed FE model is reliable. The FE model developed in this research was able to simulate well the strength capacity of in-situ cast sandwich panels subjected to eccentric compression loading. The model represented well these panels composed of two layers of reinforced concrete with wire meshes, reinforcement steel bars, and an EPS insulation layer.

Figure 11 presents a comparison between the experimental failure mode of test specimen WP16.2 and the results obtained from the numerical model. In this observation, it can be seen that one face of the panel is predominantly under compression, while the other is under tension. It can be observed that the FE model adequately simulated the behavior of the sandwich panel after failure. The results show concrete cracking due to tension in the region near the mid-height of the panel. This cracking pattern is associated with the curvature near the mid-height of the panel, which is typical of the buckling mode produced by the eccentric compression loading.

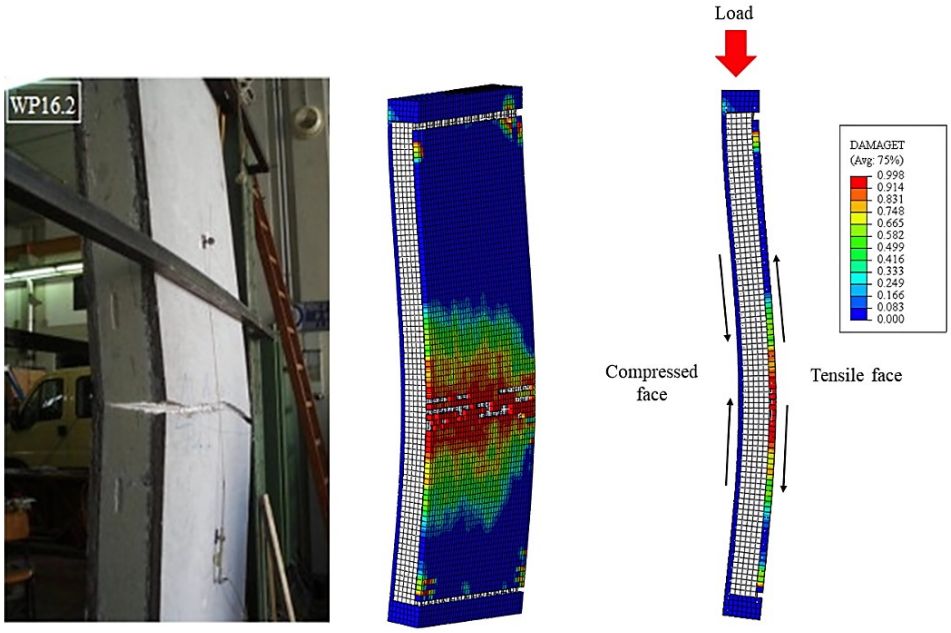


**Figure 11.** Mode of failure of the experimental and numerical models.

In Figure 12, the stress distribution in the steel of the wire meshes, connectors, and end beam reinforcements is presented at the moment of panel failure. It can be observed that the connectors do not reach the yield stress ($\sigma_y$ = 600 MPa). However, upon analyzing the region where concrete cracking takes place, it can be seen that in this region connector buckling can be noticed. The phenomenon is attributed to the compressive force exerted by the compressed layer of the panel, which pushes the connectors onto the tensile layer, as illustrated in the detail indicated in Figure 12.

Still focusing on the stress distribution in the connectors in Figure 12, it is possible to observe in the upper third region of the panel that the connectors undergo a rotational movement. The end of the connector attached to the tensioned face moves downward, while the other end attached to the compressed face moves upward. This movement occurs due to the relative sliding between the outer concrete layers of the panel, caused by the buckling mode imposed by the eccentric loading and the pin support (roller) – see Figure 3.

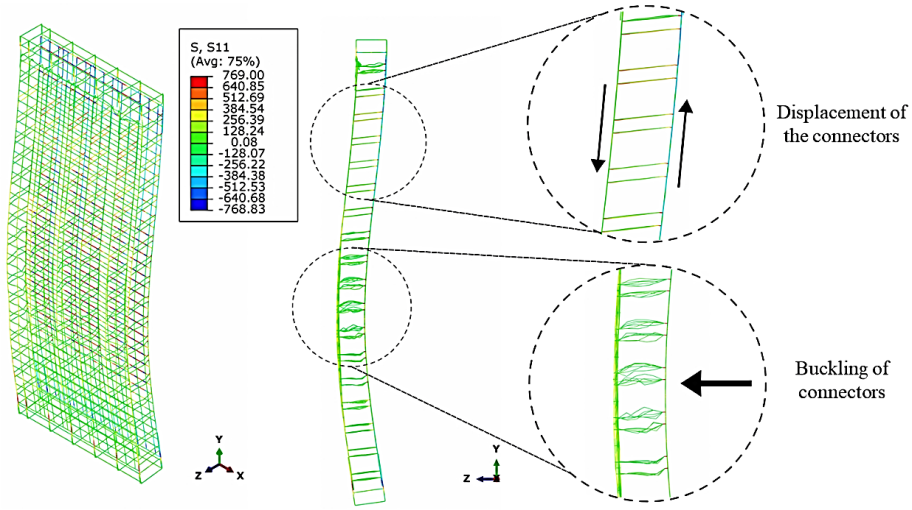


**Figura 12.** Stress distribution (in MPa) in the steel at the moment of failure.

In light of the foregoing, it can be asserted that the panel failure is due to the buckling of connectors and concrete cracking due to tension in the region near the panel's mid-height. The panel there exhibits a curvature typical of buckling resulting from the eccentric compressive loading applied at the top Figure 3. Thus, the numerical model successfully captured the behavior of the sandwich panel post-failure, as evidenced by its agreement with the experimental model's failure mode. Notably, the same failure mode was observed in the numerical models of both WP08 and WP12 panel types, as illustrated in Figure 13.

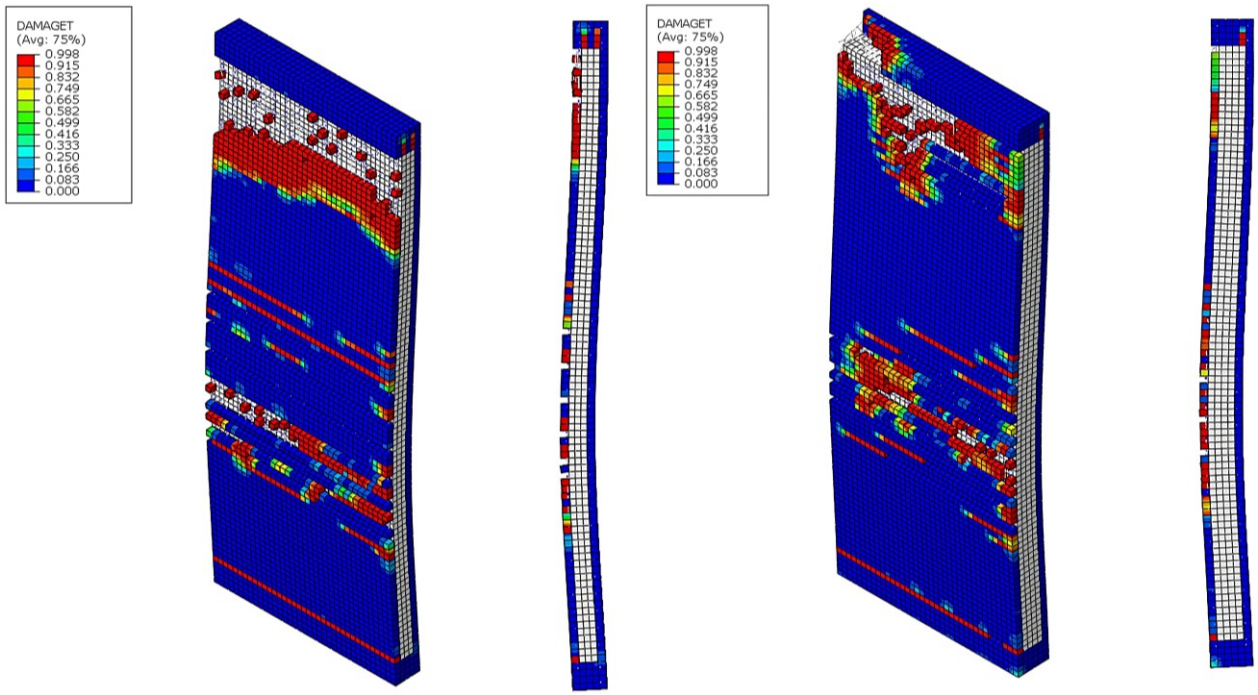


**Figura 13.** Rupture mode of panels WP08 and WP12.

The relative slipping and separation between the concrete layers of the sandwich panels were also analyzed in the experimental models by measuring vertical and horizontal displacements in both layers at the upper mid-third height of the panel using transducers. Figure 14 presents the experimental results obtained from test specimen WP08.2 for the slipping and separation between the layers, along with the results provided by the numerical model.

Figure 14 shows the slipping and separation between the concrete layers. Analyzing this figure, a good correlation of the results can be identified, especially among the curves representing the separation between the concrete layers. Thus, the FE model successfully simulated the relative displacements between the layers of the sandwich panel. In Figure 15, these results can be observed for the other numerical models, where a

similar trend was observed for all panels, showing an increase in displacements as the thickness of the insulation layer is increased.

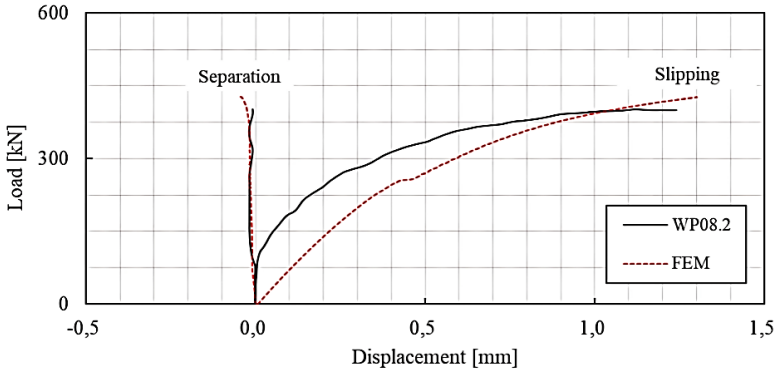


**Figure 14.** Slipping and separation between the concrete layers.

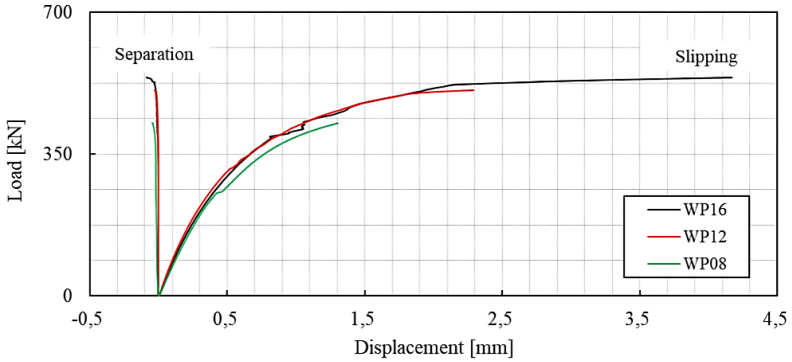


**Figure 15.** Slipping and separation between the concrete layers for the numerical models.

Another aspect analyzed in the research of Gara et al. (2012) was the vertical deformation in the two concrete layers, using displacement transducers in a strain gauge configuration positioned at the mid-height of the panel. The results for the test specimen WP08.2 are presented in Figure 16, along with the curves obtained from the numerical model, where $S_{vf}$ and $S_{vb}$ refer to the vertical displacements measured at the front and back faces of the panel, respectively.

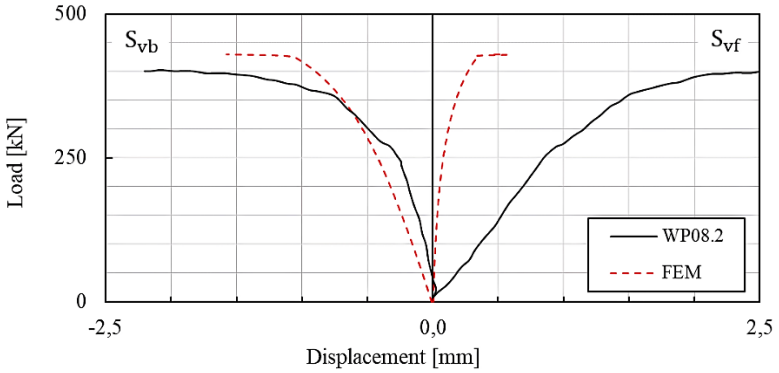


**Figure 16.** Vertical deformation in the concrete layers.

Figure 16 presents the vertical deformation in the concrete layers. Examining this figure, it can be assumed that the experimental model (Gara et al., 2012) exhibits behavior characterized by shortening deformation in the concrete compression layer and elongation deformation in the tension layer. The numerical model effectively simulates the shortening deformation of the compression layer. However, there is a discrepancy in the results for the elongation deformation of the tension layer, where the numerical model demonstrates higher stiffness. This behavior may be attributed to the modeling technique applied here to model the wire meshes. The wire mesh modeling does not take into account the real stiffness of the welded connection, in particular the welds at the intersections between transverse and longitudinal steel wires and connectors.

Therefore, the modeling technique employed enhances the stiffness of the wire mesh by disregarding the fragility zones of the welded connections. In the experimental model by Gara et al. (2012), the wire mesh rupture at the weld near the cracked region in the tensile layer occurs. However, the numerical model was unable to replicate this rupture. With a stiffer wire mesh, a reduced opening of cracks in the tensile layer is observed, leading to a decrease in the elongation deformation of the concrete layer. Figure 17 plots the load-vertical deformation curves for the numerical models of the three panels under analysis in this study. These graphics show that all panels behave in the same way, as also observed in Figure 16.

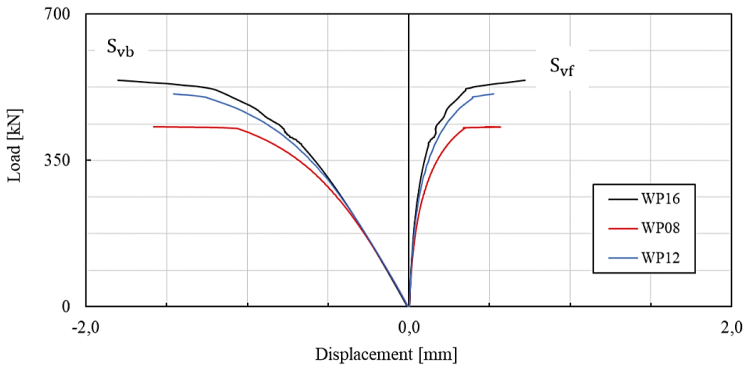


**Figure 17.** Vertical deformation in the two concrete layers for the numerical models.

Another important aspect that should be mentioned is the fact that the contact interactions between the EPS core and the concrete layers did not show a significant influence on the numerical results depicted in Figure 16 and Figure 17. This outcome can be attributed, as discussed earlier, to the substantial stiffness difference between the concrete layers and the insulation layer, such that the EPS core does not contribute significantly to the shear transfer between the concrete layers.

Finally, it can be stated that the numerical model developed in this study provides more accurate results than those obtained using simplified two-dimensional models commonly found in the literature, such as the numerical model presented in the research by Gara et al. (2012). The three-dimensional model enabled a detailed analysis of the internal structure of the panel and revealed that the failure mode occurred due to the buckling of the connectors. This level of detail could not be investigated using the simplified numerical model developed by Gara et al. (2012), which employs spring elements to simulate the connectors of the panel.

## Conclusion

The scope of this research was limited to a specific type of in-situ molded sandwich panel consisting of two layers of reinforced concrete with welded steel wire meshes and a rigid EPS insulation layer between the concrete layers. The connection between the concrete layers was achieved through straight steel connectors, whose ends were welded to the wire meshes. The primary application of this type of panel is in wall construction. The main objective was to assess the structural behavior of these panels under compression loads, and for that purpose, a nonlinear 3D finite element model was developed using ABAQUS software. The model aimed to simulate the experimental tests conducted by Gara et al. (2012), who performed six eccentrically compression tests on wall sandwich panels with different insulation layer thicknesses.

The numerical model was validated by analyzing various aspects of the structural behavior of three sandwich panels (WP08, WP12, and WP16) from the experimental tests. A good correlation was observed between the load-lateral deflection curves of the experimental and numerical models, with an average value of 0.987 for the ratio between the failure loads of the experimental and numerical models and a coefficient of variation of 0.113. These results demonstrate a satisfactory representativeness.

Furthermore, the comparison between the failure modes of the WP16 panel and the FE model also showed that the numerical model effectively reproduces the components of the sandwich panels. This enables detailed stress analysis of the internal structure, as demonstrated in the evaluation of the failure modes. With the FE model, it was possible to accurately identify the stress distribution in the concrete layers and the reinforcements of the panel, as well as the occurrence of buckling in the connectors.

Based on the obtained results, it was concluded that the failure of the panel occurs due to the buckling of the connectors and by the cracking of the concrete due to tensile stress in the region near the mid-height of

the panel. The characteristic curvature of the buckling, resulting from the eccentric compression loading, confirms this behavior. Both the numerical model and the experimental model of Gara et al. (2012) presented this buckling phenomenon in a similar manner. Thus, it can be stated that the FE model effectively reproduces the behavior of sandwich panels after failure.

The structural behavior of the sandwich panels was also evaluated through the comparison between the load-slipping and separation curves of the concrete layers. This comparison showed a good correlation between the experimental and numerical results, particularly in the curves representing the separation between the concrete layers. Therefore, the FE model demonstrated good performance in simulating the relative displacements between the layers of the sandwich panel.

Another parameter analyzed was the vertical deformation between the layers of the sandwich panel. A good agreement between the experimental and numerical results was observed for the shortening deformations in the compressed layer. However, a certain discrepancy was observed in the results regarding the stretch deformation of the tensile layer. However, the results showed a slight discrepancy in the stretch deformation of the tensile layer. This discrepancy can be attributed to the slightly greater stiffness of the FE model. The FE modeling did not consider the real complexity of the welded connections present in the experimental model. Consequently, in the numerical FE results, there is less crack opening in the tensile layer. This led to a lower elongation deformation in the FE results.

Therefore, it can be concluded that the FE model developed in this study effectively simulates the structural behavior of sandwich panels subjected to eccentric compression loads, providing reliable estimates of their strength capacity and assisting in analyzing the feasibility of future experimental studies.

## References

ABAQUS. (2020). *Abaqus documentation*. Dassault Systèmes Simulia Corp.

Alfarah, B., López-Almansa, F., & Oller, S. (2017). New methodology for calculating damage variables evolution in plastic damage model for RC structures. *Engineering Structures*, *132*, 70–86. https://doi.org/10.1016/j.engstruct.2016.11.022

Angiolilli, M., & Gregori, A. (2020). Triplet test on rubble stone masonry: Numerical assessment of the shear mechanical parameters. *Buildings*, *10*(3), Artigo 49. https://doi.org/10.3390/buildings10030049

Benayoune, A., Samad, A. A. A., Trikha, D. N., Abang Ali, A. A., & Ashrabov, A. A. (2006). Structural behaviour of eccentrically loaded precast sandwich panels. *Construction and Building Materials*, *20*(9), 713-724. https://doi.org/10.1016/j.conbuildmat.2005.02.002

Bertini, A. A., & Pinheiro, L. M. (2007). Análise experimental de painéis tipo sanduíche à flexão. *Cadernos de Engenharia de Estruturas (USP)*, *9*, 1–28.

Bezerra, L. M., Barbosa, W. C. S., Bonilla, J., & Cavalcante, O. R. O. (2018). Truss-type shear connector for composite steel-concrete beams. *Construction and Building Materials*, *167*, 757-767. https://doi.org/10.1016/j.conbuildmat.2018.01.183

Chen, A., Norris, T. G., Hopkins, P. M., & Yossef, M. (2015). Experimental investigation and finite element analysis of flexural behavior of insulated concrete sandwich panels with FRP plate shear connectors. *Engineering Structures*, *98*, 95-108. https://doi.org/10.1016/j.engstruct.2015.04.022

Clementi, F., Gazzani, V., Poiani, M., Mezzapelle, P. A., & Lenci, S. (2018). Seismic assessment of a monumental building through nonlinear analyses of a 3D solid model. *Journal of Earthquake Engineering*, *22*(1), 35-61. https://doi.org/10.1080/13632469.2017.1297268

Cornelissen, H. A. W., Hordijk, D. A., & Reinhardt, H. W. (1986). Experimental determination of crack softening characteristics of normal weight and lightweight concrete. *Heron*, *31*(2), 45–56. https://heronjournal.nl/31-2/6.pdf

Feenstra, P. H., & de Borst, R. (1993). Aspects of robust computational modeling for plain and reinforced concrete. *Heron*, *38*(4), 1–76. https://heronjournal.nl/38-4/1.pdf

Fédération Internationale du Béton [FIB]. (2013). *fib Model Code 2010: Final draft – Volume 1*. International Federation for Structural Concrete.

Gara, F., Ragni, L., Roia, D., & Dezi, L. (2012). Experimental tests and numerical modelling of wall sandwich panels. *Engineering Structures*, *37*, 193-204. https://doi.org/10.1016/j.engstruct.2011.12.027

Goh, W. I., Mohamad, N., Abdullah, R., & Abdul Samad, A. A. (2016). Finite element analysis of precast lightweight foamed concrete sandwich panel subjected to axial compression. *Journal of Computer Science & Computational Mathematics*, *6*(1). https://doi.org/10.20967/jcscm.2016.01.001

Hopkins, P. M., Chen, A., & Yossef, M. (2017). Static and dynamic analyses of insulated concrete sandwich panels using a unified non-linear finite element model. *Engineering Structures*, *132*, 249-259. https://doi.org/10.1016/j.engstruct.2016.11.017

Huang, Q., & Hamed, E. (2019). Nonlinear finite element analysis of composite precast concrete sandwich panels made with diagonal FRP bar connectors. *Composite Structures*, *212*, 304-316. https://doi.org/10.1016/j.compstruct.2019.01.019

Lee, J., & Fenves, G. L. (1998). Plastic-damage model for cyclic loading of concrete structures. *Journal of Engineering Mechanics*, *124*(8), 892-900. https://doi.org/10.1061/(ASCE)0733-9399(1998)124:8(892

Lima, J. M., Bezerra, L. M., Bonilla, J., Silva, R. S. Y. R. C., & Barbosa, W. C. S. (2020). Behavior and resistance of truss-type shear connector for composite steel-concrete beams. *Steel and Composite Structures*, *36*(5), 569–586. https://doi.org/10.12989/scs.2020.36.5.569

Lima, J. M., Bezerra, L. M., Bonilla, J., & Barbosa, W. C. S. (2022). Study of the behavior and resistance of right-angle truss shear connector for composite steel concrete beams. *Engineering Structures*, *253*, Artigo 113778. https://doi.org/10.1016/j.engstruct.2021.113778

Lubliner, J., Oliver, J., Oller, S., & Oñate, E. (1989). A plastic-damage model for concrete. *International Journal of Solids and Structures*, *25*(3), 299-326. https://doi.org/10.1016/0020-7683(89)90050-4

Nguyen, H. T., & Kim, S. E. (2009). Finite element modeling of push-out tests for large stud shear connectors. *Journal of Constructional Steel Research*, *65*(10-11), 1909-1920. https://doi.org/10.1016/j.jcsr.2009.06.010

PCI Committee Report. (2011). *State of the Art of Precast/Prestressed Concrete Sandwich Wall Panels*. *PCI Journal*, *56*(2), 131–176. https://www.pci.org/PCI_Docs/Design_Resources/Misc/Sandwich%20Wall%20Panels%20Guide.pdf

Santana, P. F. M., Silva, P. C. S., Ferreira, M. P., Bezerra, L. M., & Oliveira, M. H. (2022). Experimental and numerical study of headed bars embedded in RC members under tension. *Structural Engineering and Mechanics*, *84*(6), 531–546. https://doi.org/10.12989/sem.2022.84.4.531

Serpilli, M., Clementi, F., & Lenci, S. (2021). An experimental and numerical study on the in-plane axial and shear behavior of sprayed in-situ concrete sandwich panels. *Engineering Structures*, *232*, Artigo 111814. https://doi.org/10.1016/j.engstruct.2020.111814